Visualization of Vasculature with Convolution Surfaces: Method, Validation and Evaluation

Steffen Oeltze and Bernhard Preim

***Abstract*— We present a method for visualizing vasculature based on clinical CT- or MR data. The vessel skeleton as well as the diameter information per voxel serve as input. Our method adheres to these data, while producing smooth transitions at branchings and closed, rounded ends by means of convolution surfaces. We examine the filter design with respect to irritating bulges, unwanted blending and the correct visualization of the vessel diameter. The method has been applied to a large variety of anatomic trees. We discuss the validation of the method by means of a comparison to other visualization methods. Surface distance measures are carried out to perform a quantitative validation. Distance measures between convolution surface and isosurface renderings of the segmentation result have been determined to assess the accuracy. Furthermore, we present the evaluation of the method which has been accomplished by means of a survey of 11 radiologists and surgeons.**

I. INTRODUCTION

IN medical education as well as in therapy planning, the visualization of vasculature is crucial. It is desirable that the topology of vascular trees, can be correctly inferred from the visualization. Moreover, the curvature and the diminution of the diameter towards the periphery should be depicted correctly. Traditional methods of medical volume visualization, such as direct volume rendering, threshold-based isosurface rendering, or MIP are not well-suited for the above-mentioned goals. Due to image noise and the limited resolution of computed tomography (CT) or magnetic resonance imaging (MRI) conventional methods produce noisy 3d visualizations. Also, the visual separation of contrast-enhanced vascular structures and other high-intensity structures, such as bones, might be very difficult. Artifacts and discontinuities in the visualization distract the viewer. For educational purposes and therapy planning, vascular structures should be reconstructed based on the radiological data of that patient and some model assumptions as to the shape of vasculature (Gerig et al. [1]). Furthermore, reconstructed visualization methods are useful in the vessel analysis stage because segmentation errors become obvious.

We describe a new method for vessel visualization which originates from implicit modeling. This method produces smooth surfaces even at endpoints and branchings. The vessel skeleton serves as the input for the visualization process. It is represented as a directed graph [2]. Edges of this graph are approximated by line segments connecting adjacent voxels. Each segment is described by its two endpoints and one associated radius (the radius of the largest circle completely enclosed by the segmentation result), respectively. The visualization method applied here is based on *convolution surfaces* introduced by Bloomenthal and Shoemake [3]. As a difference to previous applications of convolution surfaces we shall faithfully represent the radius distribution given by the vessel analysis.

We carefully investigate surface distances between our visualization and other visualization methods. In particular, we compare isosurface renderings of the vessel segmentation result with convolution surfaces. In an evaluation with 11 experienced medical doctors the usefulness of our method specifically for close-up views is shown.

II. PRIOR AND RELATED WORK

Following the pioneering work of Gerig et al. (recall [1]) several attempts have been made to develop special visualization techniques for anatomic tree structures in general and vascular trees in particular. Our visualization technique is based on the model assumption that cross sections of non-pathologic vessels have a circular shape, as discussed in [4]. Masutani et al. fitted cylinders along the skeleton to visualize vascular structures. The drawback of this method is that discontinuities at branchings arise where cylinders with different diameters coincide. A special problem, the visualization of cerebral structures, has been tackled by Puig et al. [5]. She modeled typical bifurcations and pathologic situations, such as aneurysms and stenosis, and fitted these models to the patient specific data at hand. The focus of her work is on the geometric continuity and on realistic shading.

In [6] a vessel visualization pipeline has been introduced. The skeleton and the local vessel diameter determined in the image analysis stage are smoothed with a (121) binomial filter. Special care is taken at branchings to weight the incident branches. In the mapping step, truncated cones are used to represent the diminutions of the vessel diameter faithfully. However, the fitting of primitives along the skeleton does not generate smooth transitions between vessel segments at branchings. In [7], branchings are treated separately to avoid rendering discontinuities and the construction of objectionable structures inside the geometric model. Along straight parts, a vessel segment is approximated by four quadrilateral patches. The method is based on the iterative refinement of a rough, initially constructed base mesh by means of subdivision surfaces. A comprehensive survey of methods for vessel visualization is given in [8].

A. *Reconstruction of Vessels for Interaction*

Not much effort was spent so far on the exploration of vascular structures. The exploration is crucial because anatomic trees are nowadays often very complex and difficult to understand at a glance. Facilities to restrict the visualization of such tree structures are essential to support the understanding.

In [9] vessels have been segmented and analyzed in order to selectively hide them. The subdivision of vessels by placing and moving balloons with the goal to interact with such parts of vascular structures is described in [10]. [11] deals with the geometrical and morphological analysis of retinal blood images. Although interaction facilities are not directly addressed they describe the determination of measurements which are useful for interaction.

III. MODELING OF TREE-LIKE STRUCTURES WITH IMPLICIT SURFACES

Implicit surfaces offer an alternative to explicitly constructing the surface of an object by a set of polygons or parametric patches. They describe the surface by an equation which is often more compact than its parametric counterpart. Especially in modeling smooth, deformable objects, implicit surfaces unfold their full strength. James F. Blinn introduced implicit surfaces in computer graphics. He developed *Blobby Molecules* to visualize electron density fields [12].

A. Implicit Surfaces: a Brief Introduction

A classical example for an implicit equation is the description of a sphere with radius r: $x^2 + y^2 + z^2 - r^2 = 0$. This formula may be used to represent all points ***p(x,y,z)*** in space which are on the surface of a sphere with radius r. Furthermore, it facilitates point classification by simply checking the sign of the resulting scalar value. The above equation can be rewritten as Eq. 1:

$$F(p) - Iso = 0 \tag{1}$$

$F(p)$ is called the *scalar field function* because a scalar value may be computed for each point p. Iso denotes the *isovalue* for generating an *isosurface* which represents the surface where the implicit equation is zero. In order to create more complex objects, several points might be specified whose scalar fields overlap if close enough.

The scalar field function employed for modeling 'blobs' [12] is given in Eq. 2:

$$F(p) = be^{-\sigma d^2} \tag{2}$$

where d is the Euclidean distance between point p and the center c_e of an electron. Eq. 2 describes a Gaussian bump centered at c_e, having height b and standard deviation σ. For several energy sources, the scalar value at p can be calculated as Eq. 3:

$$F(p) = \sum_i b_i e^{-\sigma_i d_i^2} \tag{3}$$

Note that only scalar fields around point primitives were considered so far.

B. Convolution Surfaces

Bloomenthal and Shoemake extended the concept to skeletal primitives of theoretically any kind, e.g. line segments, polygons, or planar curves [3]. This enhancement overcomes a major drawback of point primitives namely their deficiency in describing flat surfaces and smooth generalized cylinders. They introduce *convolution surfaces* to model the surface of an object around its skeleton. In the following, S denotes a skeleton and s refers to a single point on the skeleton.

With *convolution surfaces* the scalar value is calculated according to Eq. 4:

$$F(p) = f(S,p) = \int_S \left(e^{\left(\frac{-\|s-p\|^2}{2} \right)} \right) ds \tag{4}$$

where $f(S,p)$ is the convolution of a skeleton with a three-dimensional Gaussian filter. In contrast to other implicit surfaces, the value is computed considering *all* points of the skeleton by integration. The resulting surface does not show creases and is bulge-free for non-branching skeletons.

Convolution surfaces utilize a concept which is well known from signal processing namely the modification of a signal by a filter. For a Gaussian filter function with height 1 and standard deviation $1/2$, Eq. 4 may be rewritten as

$$F(p) = f(S,p) = (h \otimes S)(p) \tag{5}$$

where S is the signal, h is the filter function and $\otimes$ denotes the convolution operator. For the visualization of vasculature, the vessel skeleton corresponds to the signal. The selected filter function should smooth this signal and thereby letting high frequencies gently drop off in the neighborhood. The resulting field around the skeleton corresponds to the scalar field mentioned earlier. By constructing an isosurface through this field the convolution surface is formed.

For the understanding of bulge-free blending it is necessary to elaborate on the superposition property of convolution:

$$h \otimes (S_1 + S_2) = (h \otimes S_1) + (h \otimes S_2) \tag{6}$$

> This guarantees, for example, that two abutting, collinear segments [...] produce the same convolution as does the single segment that is their union. [13]

Furthermore, superposition has an impact on implementation issues and the modeling process. It permits the convolution of a complex object primitive by primitive in an arbitrary order instead of considering the skeleton as a whole.

C. Filter Selection

An appropriate filter function should be continuous and monotonic. Furthermore, it should have finite support (or be negligible beyond a certain distance), and exhibit zero or near zero gradient at this distance. These requirements restrict the filter selection to low-pass filters. The Gaussian is a prime example for such filter functions. Numerous other kernels have been published. [14] includes an analysis of widespread functions with respect to computational complexity and the types of modelling primitive. For the visualization of anatomic tree structures each of the surveyed kernels is applicable. However, the scope of eligible filter functions is strongly reduced when a convolution surface should faithfully represent a given radius distribution.

Initially, the convolution surface along a line segment has a fixed radius. In [14], the creation of a surface that resembles a tapered cylinder by using linear profiling functions is described. The use of Bezier curves with two control points for representing linear radius distributions is introduced in [15]. Both methods are convenient when interactive radius modification is required. However, they are inadequate for modeling surfaces that exactly converge against a given radius. As far as we know, solely in [13] and [16] approaches have been published that concentrate on this problem.

In [13] a Gaussian function is utilized for convolution:

$$h(p) = e^{-d(p,S)^2\omega},\ \omega = \ln 2,\ d(p,S) > 0 \tag{7}$$

where ω is referred to as the *width coefficient* which equals $1/(2\sigma^2)$. The distance between point p and the line segment skeleton S is denoted by $d(p,S)$.

In [16] the use of two other filter functions is discussed with regard to the correct representation of a linear radius distribution. However, both the suggested inverse cubic function ($1/d(p,S)^3$) as well as an alternative function ($r^2/d(p,S)^2$, where r equals the varying radius along the line segment) decrease more slowly to near zero compared to the Gaussian.

1) Discussion: Computational speed determined our choice of a filter function. By definition of the convolution surface (Eq. 4), the entire skeleton needs to be considered when calculating the scalar value at a point p. For the visualization of vascular structures this means a prohibitively high computational effort. To improve the performance, we will restrict the computation of the scalar field using bounding volumes along line segments. The tightness of a suitable bounding volume strongly depends on the filter function, in particular on the distance from the center where the function value is negligible. We choose the Gaussian because it drops much faster to zero than the other two kernels discussed in [16]. In [17], the filter selection is discussed in more detail.

D. Correct Representation of the Radius Distribution

According to [13], the computation of the convolution integral in Eq. 4 may be simplified by separating it into the product of the *integration filter* and the *distance filter*. Whereas the first term requires solving a one-dimensional integral the second is simply a single evaluation of the kernel:

$$h(p) = e^{-(d(p,H))^2\omega}, \tag{8}$$

where $d(p,H)$ is the distance between point p and its projection H on the line which proceeds through the considered line segment (if p is near the end of the segment, H might be beyond the segment). The separation of the computation into two filters is crucial for the evaluation of the implicit function. Instead of the 3d integration (Eq. 4) we have to solve a 1d integral which can be precomputed and stored in a lookup table. We use the same lookup table as [13] with 10000 entries.

For adapting the radius of the resulting convolution surface, $d(p,H)$ is divided by radius $r(H)$. Latter is determined with linear interpolation between the radii at the segment endpoints. In order to let the convolution surface converge against a desired radius, an appropriate isovalue and a width coefficient ω must be selected. Bloomenthal employed an isovalue of $1/2$ so as to let the convolution surface pass through the segment endpoints. Now, let us consider the convolution surface of a sufficiently long cylinder and a point p which is located exactly on the surface and in the middle of it. Here, the integration filter equals 1 since the kernel is fully subtended by the segment. With the constraint that $d(p,H) = r(H)$ for point p on the convolution surface it follows:

$$F(p) = e^{-(r(H)/r(H))^2\omega} - 1/2 = e^{-\omega} - 1/2 = 0 \tag{9}$$

Thus, $\omega = \ln 2 \approx 0.6931$.

IV. BLENDING

The creation of smooth transitions between simple objects intending to form a complex organic shape is a strength of implicit surfaces. Here, so-called *blends* are used instead of parametric free-form surfaces. For convolution surfaces, blending corresponds to an integration of the filter along the entire skeleton. At the skeleton joints, the scalar fields of adjacent primitives overlap. The convolution surface constructed through the resulting field forms a smooth envelope of the underlying joint. In an implementation, each primitive may be convolved separately due to the superposition property of convolution. Blending may also have negative effects for a faithful visualization of anatomic tree structures which are discussed in the following.

A. Blending Strength at Branchings

With the initial filter design in [13], the transitions at branchings were very smooth but deviated strongly from the skeleton. Discussions with an experienced radiologist showed that this is undesirable and in some cases the interpretation of the topology is even hampered. We propose a narrower filter kernel which results in a surface which tracks the skeleton more faithfully.

B. Unwanted Blending

For precise modeling of complex shapes it is essential to control the blending between certain parts of the object. Concerning vascular structures, vessel segments whose skeleton is not connected should not blend with each other. In [18] a *restricted blending graph* was suggested to overcome this problem. Based on the topology of the given skeleton, primitives are classified into blending-groups of the following types: all primitives blendable, all primitives unblendable, blendable and unblendable primitives. Unfortunately, this solution does not ensure C^1 continuity of the shape. A more recent approach [19] introduces *local convolution*. This concept is based on defining a restricted skeleton range for computing the scalar value at a certain point in space. It prevents blending even between small folds of the skeleton.

C. Bulging

Convolution surfaces are bulge-free for non-branching line segment skeletons due to the superposition property of convolution. However, as shown in [13], they do exhibit bulges at branchings. This effect is disturbing for the visualization of vascular structures since a bulge might be easily mistaken for a pathological variation, e.g. an aneurysm. Even though our visualization method is not targeted at supporting vascular diagnostics, we shall minimize this drawback.

D. Consequences

As a consequence of our analysis of different filters we choose the Gaussian [13] for the convolution. However, we suggest a modification of the original kernel to reduce the blending strength at branchings. Employing the altered filter function has an impact not only on the blending strength but also on the unwanted blending problem as well as the bulging problem. Furthermore, with the modified filter function the polygonization of scalar fields might be accelerated by means of tighter bounding volumes.

V. VISUALIZATION OF ANATOMIC TREE STRUCTURES WITH CONVOLUTION SURFACES

In this section we describe how a modified width coefficient allows to solve the blending problems. We go on and discuss a preprocessing of the data in order to reduce the effort to compute the convolution surface. The same vessel analysis results which have been used in [6] are the input for our method. We also employ the binomial filtering to smooth the vessel skeleton and diameter.

A. Filter Modification

We carefully evaluated different width coefficients using a variety of datasets and found that a value of $\omega = 5ln(2)$ is suitable to prevent the undesired effects such as unwanted blending and bulging. Note, that the width coefficient has been increased with the effect that the filter function is narrower. In order to correctly represent the radius distribution along a line segment, a recalculation of the isovalue is required. Under consideration of our new width coefficient the isovalue (Iso) is evaluated as follows:

$$F(p) = e^{-(r(H)/r(H))^2 5 \ln 2} - Iso = e^{-5 \ln 2} - Iso = 0 \quad (10)$$

Hence, $Iso = 1/32 = 0.03125$.

To evaluate our filter function, we employ a simple skeleton with a trifurcation (4 coinciding branches). In anatomic tree structures, we never found more branches coinciding. In Fig. 1 it is illustrated how the blending strength is reduced for the simple skeleton. Also, the bulging problem is avoided with the modified filter function (see Fig. 2). To study unwanted blending, we use an S-shaped skeleton with 3 mm distance between the horizontal lines. The radius was increased until the problem occurred. With the original filter, unwanted blending appeared for a radius of 1.07 mm, whereas with the modified width coefficient, it appeared at 1.37 mm. The ratio between the distance of the convolution surfaces and the distance of the centerlines determines the occurrence of unwanted blending. With the modified width coefficient, we could reduce the ratio from 29% (see Fig. 3 (left)) to 9% (see Fig. 3 (right)).

B. Computational Complexity

For the construction of the convolution surface it is necessary to evaluate the scalar value at numerous points in space. Each of these computations requires considering the whole tree. By contrast to previous applications of convolution surfaces with small to moderate-sized structures vascular trees may well have more than 1000 branchings.

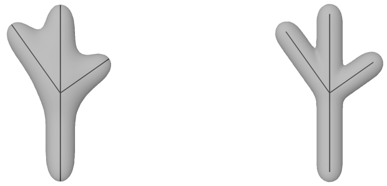

Fig. 1. Transition at branching, left: convolved with original filter function ($\omega = ln(2)$), right: convolved with modified filter ($\omega = 5ln(2)$). The semitransparent visualization reveals the underlying skeleton. Note that the original filter was designed to let the convolution surface pass through the segment endpoints. With the modified filter the surface tracks the skeleton more closely.

Fig. 2. Side view of the branching in Fig. 1. The bulging problem (left) is considerably reduced with the modified filter (right).

Fig. 3. Unwanted blending, Distance between the horizontal branches of the S-shapes is 3 mm. The radius of all branches is 1.07 mm. Unwanted blending (left) is considerably reduced with the narrower filter (right).

In order to accelerate the computation, we determine which line segments have a significant influence on a point and neglect the influence of the remaining segments. For this purpose, a partitioning of space is necessary. The voxel grid of the underlying data may be used as a basis for the partitioning.

The preprocessing proceeds as follows: While iterating over all line segments, a cylindrical bounding volume (CBV) is constructed. The cylindrical shape of the bounding volume allows to closely approximate the shape of the convolution surface and the underlying scalar field. The radius of the CBV is based on the maximum radius along the line segment and a factor computed with respect to the width of the convolution filter. The width influences the extension of the scalar field about a line segment. Although, the modified Gaussian from Sect. V-A has infinite support a factor of 1.5 has been computed as adequate for enclosing the significant part of the scalar field. The CBV is then employed to identify those voxels which are influenced by the scalar field of the current line segment (see Fig. 4). This information is used during surface construction for determining the line segments with a significant influence on a point.

The details of the acceleration are described in [17]. As a

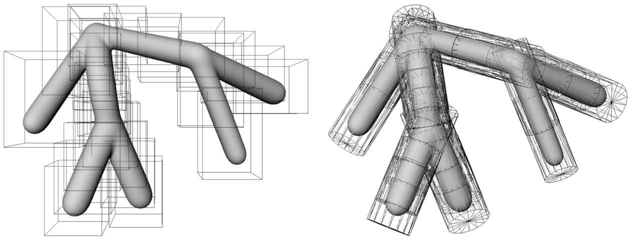

Fig. 4. Axes-aligned bounding boxes (left) and cylindrical bounding volumes (right) for an artificial tree (right)

result, the use of the CBV accelerates the whole computation by two orders of magnitude (factor 100-200).

VI. EXPLORATION OF VASCULATURE

It is often desirable to restrict the visualization of anatomic tree structures or to focus it on certain subtrees. For example, in tumor surgery, vessel segments around the tumor are more important than more distant parts. In general, surgeons would like to know which vessel segments must be reconstructed, if they have to be cut (those with a diameter above 5 mm). The vessel analysis results allow for interactions to support such visualization goals. Based on the branching graph, vessel segments which depend on a user-selected branch might be highlighted or removed from the visualization. Using a region-selection (called lasso selection), an arbitrary subset of vessels might be selected based on their position in the viewport. Instead of completely removing the selected edges it is often useful to show them less focused using gray colors and/transparency (see Fig. 5). Since the construction of polygons inside the vessel tree is avoided by applying convolution surfaces a semitransparent visualization without any artifacts is enabled.

Fig. 5. Lasso selection and defocused visualization of the selected vessel segments. Inside the semitransparent vessels the centerline is presented. (©Eurographics 2004, [17])

VII. VALIDATION

A crucial aspect for any visualization technique which is intended for clinical use is its validation. The underlying data (vessel centerline and local vessel diameter) are generated with the method described in [2]. With respect to the visualization of these data the validation should answer the following questions:

- Are (small) branches of the tree structure suppressed in the visualization (false negatives)?
- Are there occurrences of small branches which are not represented in the data (false positives)?
- Are there occurrences where separate branches appear as one branch?
- Is the constriction of the vessel diameter represented correctly?

These questions are relevant since the implicit modeling approach is more prone to such visualization errors than explicit methods where graphics primitives are explicitly fitted along the skeleton.

A. Qualitative Validation

We choose two different methods to answer the above questions: first we analyzed the visualization of artificial data with different branching types (e.g. with a trifurcation) and second we compared the implicit method with the method developed by Hahn et al. [6]. We refer to the first approach as convolution surface (CS)-visualization and to the latter one as truncated cone (TC)-visualization.

The tests with artificial data showed that unwanted effects could be strongly reduced. The unwanted blending problem may occur in rare cases. The comparison of both methods (Fig. 6) reveals a good correspondence. The TC-visualization produces longer branches at the leafs of the vessel tree. This is due to the construction where a half sphere is generated at the end of segments.

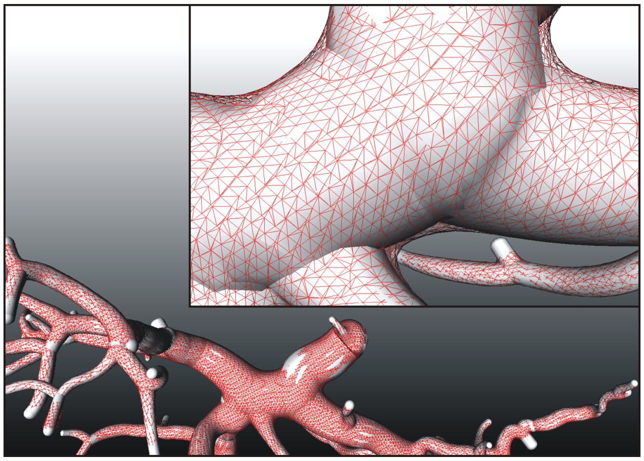

Fig. 6. The visualization method described by Hahn et al. [6] (concatenated truncated cones) and our method are combined for a qualitative validation. The convolution surfaces are rendered as wire-frame while the results of the other method are shaded. The comparison of both surfaces reveals a good correspondence.The inset illustrates that convolution surfaces form smooth transitions which diverge slightly from the truncated cones at branchings.

In order to further study the accuracy of our method, we compare it with an isosurface visualization of the vessel segmentation result (the validation of the segmentation is beyond the scope of this paper). Differences between the segmentation result and the CS-visualization can be expected because:

- the vessel diameter which guides the convolution surface is the diameter of the incircle - therefore the convolution surface underestimates the segmentation result,
- the skeleton and the vessel diameter have been smoothed and
- small side branches have been suppressed (*pruning*) during skeleton enhancement by taking into account the length of a side branch relative to the branch at the next higher level of hierarchy [6].

With respect to the four questions at the beginning of this section, we have evidence that none of the problems discussed actually occurs.

B. Quantitative Validation

Over and above the visual inspection, a quantitative analysis is desirable to judge whether the underlying data (centerline and local diameter) are faithfully represented. The validation of the vessel segmentation and skeletonization is beyond the scope of this paper. We chose to analyze the distances between surfaces constructed by isosurface rendering of the segmentation result, TC- and CS-visualization. Distance measures are most relevant here because these visualizations are often used to assess distances (e.g. from a lesion to a vessel). The measurements are carried out to describe the error that is introduced by the visualization method.

The software platform AMIRA (© Indeed - Visual Concepts GmbH, Berlin) is applied to perform a quantitative surface comparison. We compare the CS with both the isosurface and the TC. For constructing the convolution surface the width coefficient is set to $5ln(2)$ (recall Sect. V-A). A comparison is realized such that for each vertex of one surface the unsigned distance to the closest point on the other surface is computed. From the histogram of these values the following statistical measures are calculated:

- mean distance (Ø)
- standard deviation from the mean distance (σ)
- root mean square distance (Rms)
- minimum distance (Min)
- maximum distance (Max)
- median of the distance (Med)
- area deviation: percentage of distance values that deviate more than a given threshold (Area)

Since distance-measures between two surfaces are non-symmetric AMIRA supports a two-sided comparison. However, the computation of measures in direction from isosurface to convolution surface distorts the overall result. Due to pruning of tiny vessel segments during skeletonization [6] these parts are missing in the CS. For some vertices of the isosurface no points exist within a small range on the convolution surface. Hence, this comparison is disregarded as well as the comparison from TC to CS. While with the first method polygons are constructed inside the model at branchings the convolution surface is hollow. For vertices of the inner polygons no points exist within a small range on the convolution surface. The resulting high deviations would mislead the overall comparison.

The averaged results of a quantitative comparison between the surfaces of 10 different datasets based on CT of the human liver are presented in Table I. We chose half the diagonal voxel size ($VoxDiag2$) as the threshold for computing the area deviation (last column in Table I). Boxplots illustrating the distribution of measured distances for each dataset are presented in Fig. 7.

TABLE I

AVERAGED RESULTS OF THE QUANTITATIVE COMPARISON OF SURFACES BASED ON 10 DIFFERENT DATASETS. MEASURES WERE COMPUTED FROM CS TO ISOSURFACE (ISO) AND FROM CS TO TC. ALL LENGTH MEASURES ARE IN mm WHEREAS AREA IS MEASURED IN %.

	Ø	σ	Rms	Min	Max	Med	Area
CS→Iso	0.37	0.32	0.49	0	3.21	0.29	8.74
CS→TC	0.09	0.10	0.14	0	1.07	0.05	0.22

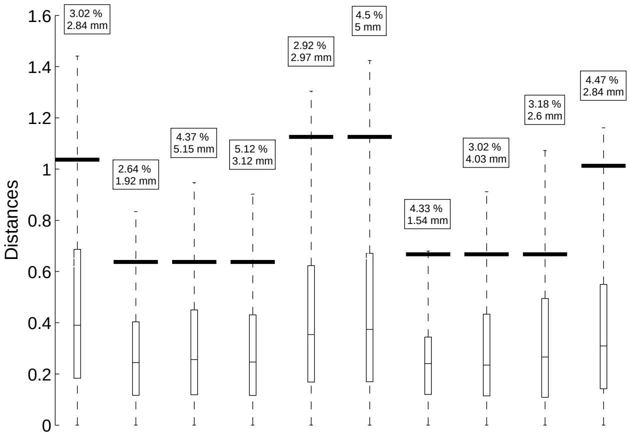

Fig. 7. Boxplots of the distance measures (in mm) carried out for a comparison of CS and Isosurface based on 10 different datasets. Each box has lines at the lower quartile, median, and upper quartile values. The whiskers extend from each end of the box to show the extent of the rest of the data. Their length corresponds to the inter-quartile range multiplied by 1.5. The upper value within each text box represents the percentage of data values beyond the ends of the whiskers. The lower value is the maximum distance. Thick lines indicate the $VoxDiag2$ values. Note that each upper quartile is consistently below its corresponding value.

With an average of 0.37mm deviations between convolution surface and isosurface are below a typical value for $VoxDiag2$. Note, also the average area overlap of 91.26% which refers to the respective value of $VoxDiag2$. It could be observed that high deviations (> 3mm) occur in all datasets only close to the root of the vessel tree as illustrated in Fig. 8. This effect is negligible because the root does not pertain to the intrahepatic vessel system and is therefore of less interest for surgery planning. Inside the vascular trees even distance measurements are reliable with the CS. The median of the deviation is below $VoxDiag2$ for each considered dataset. The deviations along the whole vessel tree are to be expected since the convolution surface constantly underestimates the segmentation result as described in Sect. VII-A. It could be further ascertained that smoothing the vessel skeleton has a negligibly small effect on the measurements. The convolution surfaces based on their corresponding non-smoothed skeletons yielded almost the same results. Pruning of small side branches has no effect since the surface comparison is only accomplished from convolution surface to isosurface and not vice versa.

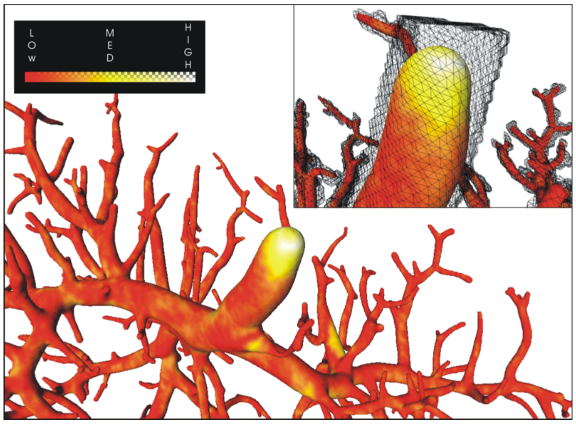

Fig. 8. Color-coded visualization of the deviation from convolution surface to isosurface. Each vertex of the convolution surface is assigned a color with respect to the corresponding distance. The legend represents the correlation between color and magnitude of the deviation. The strongest deviations occur at the root of the vessel tree as depicted in the inset showing the superimposed isosurface in wire-frame mode.

As could be expected there is a better correspondence between the two model-based approaches (TC- and CS-visualization). More than 99% of the directional distances are below $VoxDiag2$. The average maximum deviation between CS and TC is 1.07mm, which is less than a typical diagonal voxel size. The low deviations indicate that strong blending, unwanted blending and bulging are effectively avoided. The CS represents the vessel skeleton and diameter as faithful as the TC. The computational results reveal that the deviation from CS to TC ranges from $0mm$ up to $1.07mm$. Minor deviations are observed at the branchings which results from the smooth transitions of the convolution surface (Fig. 9). These naturally diverge slightly from the discontinuous transitions of the polygonal model built according to the TC-visualization. Along straight parts of the vessel tree both surfaces almost perfectly coincide. The highest deviations occur at the vessel ends since the TC-visualization produces longer branches at the leafs of the vessel tree (recall Sect. VII-A).

VIII. Evaluation

To evaluate the benefit of our method, we prepared a survey in order to compare it to other visualization methods. For this purpose a collection of visualization results was rated by six experienced surgeons and five radiologists (1 woman, 10 men). All participants in the study had experience with 3d visualizations and in particular with the visualization developed by [6].

The collection represented three different liver vessel trees from CT data and consisted of 10 images per tree: one context view for better orientation showing the tree within the liver lobe and three different close-ups generated by isosurface rendering, TC- and CS-visualization, respectively. The viewing direction as well as all other visual parameters are identical (Fig. 10).

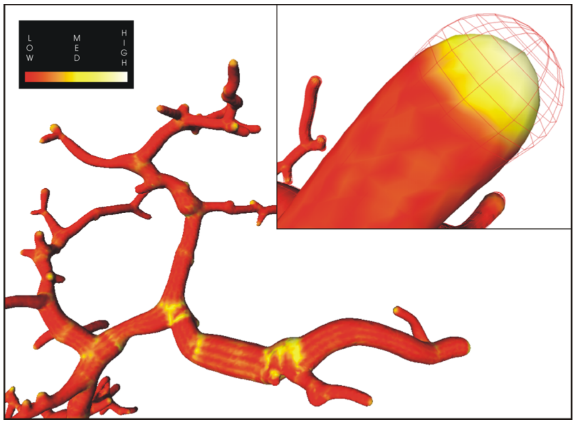

Fig. 9. Color-coded visualization of the deviation from convolution surface to the surface constructed by means of truncated cones [6]. Minor deviations may be observed at the branchings. The strongest deviations occur at the vessel ends as illustrated in the inset. Here, the superimposed truncated cones caped by a hemisphere are rendered in wire-frame mode.

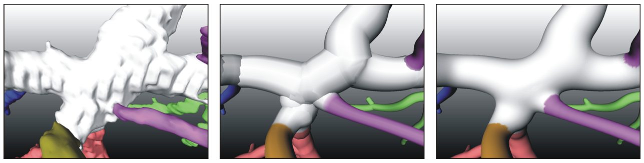

Fig. 10. Close-ups of a liver vessel tree generated by isosurface rendering, concatenation of truncated cones [6] and convolution surfaces (from left to right).

The evaluation focussed on close-up views because these are relevant for therapy and surgery planning. The evaluation criteria were:

- clarity of the visualization,
- comprehensibility of spatial relations,
- similarity to operative views
- and visual quality.

For each criterion users were asked to rate from 1 (unsatisfactory) to 5 (excellent). The evaluation results are summarized in Table II.

TABLE II

Subjective Comparison of vessel visualization by isosurface rendering (Iso), TC and CS. Ø denotes the mean value and σ represents the standard deviation. Valuations range from 1(unsatisfactory) to 5 (excellent).

	Clarity (n=11)		Comprehensibility (n=11)		Similarity to operative views (n=8)		Visual quality (n=11)	
	Ø	σ	Ø	σ	Ø	σ	Ø	σ
Iso	1.8	0.69	1.9	0.85	1.6	0.7	1.7	0.69
TC	3.7	0.84	3.9	0.86	3.5	0.9	3.8	0.71
CS	4.1	0.87	4.1	0.89	4.0	0.89	4.2	0.76

Three radiologists could not compare the visualization results with operative views and therefore left this field blank. According to the outcome of the evaluation, the CS consistently achieves the best results. Even if the difference to TC is statistically not significant it reveals the potential of the CS.

Above all the similarity to operative views (column 3) and the visual quality (column 4) has been emphasized by doctors under discussion.

Furthermore, the results in Table II argue for the reconstruction of a vessel model from the segmented data. The model-based visualization (rows 2 and 3) clearly outperforms the direct visualization by isosurface rendering.

IX. RESULTS

Our method has been applied to 25 clinical datasets so far. In Fig. 11 we compare the visual quality of our method with the TC-visualization. Other examples for the visual quality of the visualization can be seen in Fig. 12-13. The visualizations do not exhibit any of the unwanted effects. We carefully examined the surfaces near branchings and noted that geometric continuity was achieved for all kinds of branchings and branching angles. The surfaces are terminated at leafs of the anatomic trees with a rounded appearance which is a consequence of the construction method.

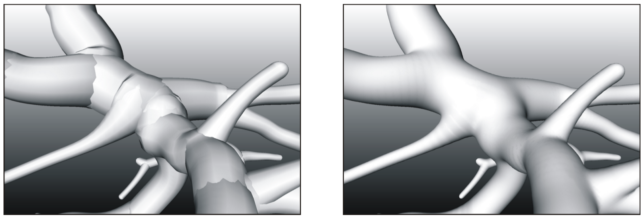

Fig. 11. Close-up of a visualization with truncated cones with artifacts along the seams (left). Smooth visualization with implicit functions of the same dataset (right).

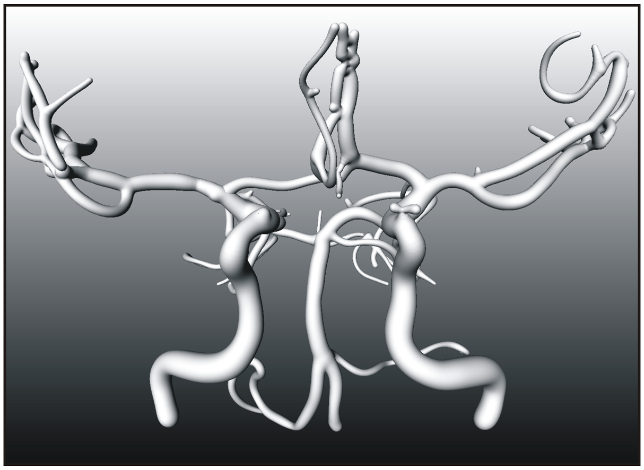

Fig. 12. Visualization of cerebral blood vessels derived from a clinical MR angiography with 149 edges.

To give an idea of the complexity of the resulting geometry and the timings involved in the computation, we present some results in Table III. The setup time includes the preprocessing step. The first row corresponds to a portal vein tree of low complexity. The two middle rows represent the datasets shown in Fig. 12 and 13. The last row in Table III represents a complex anatomic tree from a corrosion cast. Interactive frame rates (>24 fps) were achieved with the first three models (rows 1-3). Due to the extreme size of the corrosion cast (row 4), the Open Inventor optimization failed which resulted in a low frame rate.

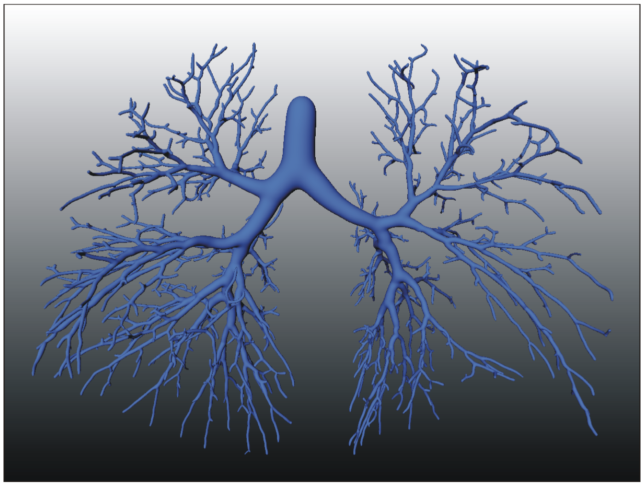

Fig. 13. Visualization of a bronchial tree derived from a clinical CT dataset with 1504 edges. (©Eurographics 2004, [17])

TABLE III

PERFORMANCE MEASUREMENTS FOR ANATOMIC TREE STRUCTURES CARRIED OUT ON A PENTIUM 4 CPU 3.2GHZ SYSTEM WITH 1024MB RAM.

edges	triangles (*1000)		setup time (s)	
	CS	Cones	CS	Cones
136	125	55	6.14	0.11
149	253	74	8.12	0.12
1504	1,126	599	53.24	1.30
3461	2,366	907	52.01	2.11

X. CONCLUSION

We have presented a method for visualizing anatomic tree structures, such as vasculature and bronchial trees, which adheres to the underlying data (skeleton and local vessel diameter), while producing smooth transitions at branchings. The method is based on convolution surfaces, a variant of implicit surfaces. The filter design has been fine-tuned to prevent irritating bulges and to represent the course of the vessel diameter faithfully. The width of the Gauss filter turned out to be the essential parameter to accomplish our visualization goals. With a preprocessing step which computes bounding volumes we can efficiently compute the convolution surface even for large vascular and bronchial trees.

We compared our new method with the TC-visualization and could show the superior visual quality. We analyzed the differences between the methods with respect to the precision and come to the conclusion that the new method faithfully represents the underlying data. The quantitative validation indicated that the convolution surfaces deviate less than $VoxDiag2$ for almost the whole dataset. The directional distances between convolution surface and isosurface rendering of the segmentation result are larger, but still below a typical value for $VoxDiag2$.

Acknowledgment

We want to thank M. Hindennach, H. Hahn and O. Konrad-Verse for providing the image analysis results on which this work is based and for fruitful discussions. We thank Prof. Terwey (Bremen), Prof. Galanski (Hannover), Prof. Kalender (Erlangen) as well as Prof. Klose (Marburg) for providing the corresponding radiological data. Furthermore, we are indebted to J. Bloomenthal for his support on theoretical and implementation aspects. We are grateful to A. Sherstyuk, A. Angelidis and S. Hornus for many enlightening conversations. We also want to acknowledge K.J. Oldhafer for exceedingly supporting the evaluation process. Many thanks go to Jeanette Cordes who did a great job in performing the quantitative validation and to Stefan Zachow for his help to efficiently use AMIRA facilities.

List of Figures

References

[1] G. Gerig, T. Koller, G. Szkely, C. Brechbühler, and O. Kübler, "Symbolic description of 3d structures applied to cerebral vessel tree obtained from mr angiography volume data," in *Proc. of Information Processing in Medical Imaging*, vol. 687. Springer, LNCS, 1993, pp. 94–111.

[2] D. Selle, B. Preim, A. Schenk, and H.-O. Peitgen, "Analysis of vasculature for liver surgical planning," *IEEE Transactions on Medical Imaging*, vol. 21, no. 11, pp. 1344–1357, Nov. 2002.

[3] J. Bloomenthal and K. Shoemake, "Convolution surfaces," *Computer Graphics*, vol. 25, no. 4, pp. 251–256, 1991.

[4] Y. Masutani, K. Masamune, and T. Dohi, "Region-growing-based feature extraction algorithm for tree-like objects," in *Proc. of Visualization in Biomedical Computing*, vol. 1131. Springer, LNCS, 1996, pp. 161–171.

[5] A. Puig, D. Tost, and I. Navazo, "An interactive cerebral blood vessel exploration system," in *IEEE Visualization*. IEEE Computer Society, 1997, pp. 443–446.

[6] H. Hahn, B. Preim, D. Selle, and H.-O. Peitgen, "Visualization and interaction techniques for the exploration of vascular structures," *IEEE Visualization*, pp. 395–402, 2001.

[7] P. Felkel, A.-L. Fuhrman, A. Kanitsar, and R. Wegenkittl, "Surface reconstruction of the branching vessels for augmented reality aided surgery," *BIOSIGNAL 2002*, vol. 16, pp. 252–254, June 2002.

[8] K. Bühler, P. Felkel, and A. La Cruz, *Geometric Methods for Vessel Visualization and Quantification - A Survey*. Springer, 2003, pp. 399–420.

[9] W. Niessen, A. van Swihjndregt, B. Elsmann, O. Wink, M. Viergever, and W. Mali, "Improved arterial visualization in blood pool agent mra of the peripheral vasculature," in *Computer-Assisted Radiology and Surgery*, H. Lemke, M. Vannier, K. Inamura, and A. Farman, Eds., vol. 1191. Amsterdam: Elsevier, 1999, pp. 119–123.

[10] D. Bartz, M. Skalej, D. Welte, and W. Strasser, "3d-virtual angiography," in *Computer-Assisted Radiology and Surgery*. Elsevier, 1999, pp. 44–48.

[11] M. E. Martinez-Perez, A. D. Hughes, A. V. Stanton, S. A. Thom, N. Chapman, A. A. Bahrath, and K. H. Parker, "Geometrical and morphological analysis of vascular branches from fundus retinal images," in *Medical Image Computing and Computer-Assisted Intervention*, vol. 1935. Springer, LNCS, 2000, pp. 756–765.

[12] J. Blinn, "A generalization of algebraic surface drawing," *ACM Transactions on Graphics (TOG)*, vol. 1, no. 3, pp. 235–256, 1982.

[13] J. Bloomenthal, "Skeletal design of natural forms," Ph.D. dissertation, Univerity of Calgary, Calgary, Alberta, Canada, 1995.

[14] A. Sherstyuk, "Convolution surfaces in computer graphics," Ph.D. dissertation, Monash University, Melbourne, Victoria, Australia, 1998.

[15] X. Jin, C.-L. Tai, J. Feng, and Q. Peng, "Convolution surfaces for line skeletons with polynomial weight distributions," *Journal of Graphics Tools*, vol. 6, no. 3, pp. 17–28, 2001.

[16] S. Hornus, A. Angelidis, and M.-P. Cani, "Implicit modeling using subdivision curves," *The Visual Computer*, vol. 19, no. 2-3, pp. 94–104, 2003.

[17] S. Oeltze and B. Preim, "Visualization of anatomic tree structures with convolution surfaces," in *Proc. of Joint IEEE/EG Symposium on Visualization*, O. Deussen, C. Hansen, D. Keim, and D. Saupe, Eds. Eurographics Association, 2004, pp. 311–320.

[18] A. Opalach and S. C. Maddock, "Implicit surfaces: Appearance, blending and consistency," in *Proc. of Eurographics Workshop on Animation and Simulation*, 1993, pp. 233–245.

[19] A. Angelidis, P. Jepp, and M.-P. Cani, "Implicit modeling with skeleton curves: Controlled blending in contact situations," in *Shape Modeling International*, ACM. IEEE Computer Society Press, 2002.